Scientific Reports

https://doi.org/10.1038/s41598-026-48296-7

Article in Press

Developing giant grass biochar-Fe_3O_4-g-C_3N_4 composite for the adsorption of methylene blue from aqueous solutions

Received: 8 December 2025

Accepted: 7 April 2026

Published online: 15 April 2026

Cite this article as: Nure J.F., Erkan H.S., Babaee S. *et al.* Developing giant grass biochar-Fe_3O_4-g-C_3N_4 composite for the adsorption of methylene blue from aqueous solutions. *Sci Rep* (2026). https://doi.org/10.1038/s41598-026-48296-7

Jemal Fito Nure, Hanife Sari Erkan, Saeideh Babaee, Mahdi Hassan, Potlako J. Mafa & Solomon Tibabu

Developing giant grass biochar-Fe_3O_4-g-C_3N_4 composite for the adsorption of methylene blue from aqueous solutions

Jemal Fito Nure[1&2*], Hanife Sari Erkan[1], Saeideh Babaee[2], Mahdi Hassan[1], Potlako J. Mafa[3], and Solomon Tibabu[4]

[1]Environmental Engineering Department, Civil Engineering Faculty, Yildiz Technical University, 34220, Davutpasa, Esenler, İstanbul, Turkey

[2]School of Chemical and Metallurgical Engineering, University of the Witwatersrand, 1 Jorissen St, Johannesburg 2000, South Africa

[3]Institute for Nanotechnology and Water Sustainability (iNanoWS), College of Science, Engineering and Technology, University of South Africa, Florida Science Campus, Johannesburg, 1710, South Africa

[4]Department of Environmental Engineering, College of Engineering, Addis Ababa Science and Technology University, 16417 Addis Ababa, Ethiopia

*Jemal Fito Nure, fitojemal120@gmail.com, ORCID-0000-0002-7770-3789

Abstract

The presence of methylene blue (MB) in textile effluents poses significant environmental and public health risks. Therefore, this study aimed to develop a giant grass biochar magnetite graphitic carbon nitride (BC-Fe_3O_4-g-C_3N_4) composite adsorbent via a co-precipitation method for the effective removal of MB from aqueous solutions. The adsorbent was characterized through proximate analysis, BET, FTIR, SEM, and pHpzc measurements. The adsorption process was evaluated considering the effects of adsorbent dose, pH, initial MB concentration, and contact time using a Central Composite Design (CCD) within Response Surface Methodology (RSM). The material characterization results showed a high fixed carbon content of 55.06%, a low ash content of 4.02%, and a BET specific surface area of 690 m^2/g. Similarly, the pHpzc was found to be 8.09, and SEM analysis confirmed a porous structure with notable surface cracks and diverse functional groups. Adsorption optimization revealed that the maximum MB removal of 93.3% occurred at an initial concentration of 100 mg/L, pH 7, an adsorbent dose of 1.25 g/100 mL, and a contact time of 72.5 min. Based on the adsorption isotherm and kinetic modeling, the experimental data closely fitted the Langmuir (R^2 = 0.99) and pseudo-second order (R^2 = 0.88) models, respectively. Regeneration studies showed the composite adsorbent was effective in the initial cycles, but performance gradually declined after three cycles. Overall, these findings suggest that the composite adsorbent has promising potential for the remediation of dye-contaminated

wastewater. However, further improvements are needed to adapt the technology for use with real industrial wastewater.

Keywords: Adsorption; composite adsorbent; dye; factorial design; water pollution; wastewater remediation

1. Introduction

Industries utilize a vast array of chemicals, generating contaminated effluents that are frequently discharged into aquatic ecosystems, leading to a significant rise in pollutant levels [1–4]. This ongoing environmental challenge results in the rapid deterioration of water quality and exacerbates global water scarcity [5,6]. Recently, top attention has been given to pollution transfer and environmental health, and the implications associated with high risk to public health due to the spatiotemporal evolution of pollution transfer in both national and local perspectives [7]. Textile industrial effluents, in particular, discharge high concentrations of dyes, which are major pollutants due to their complex aromatic structures and high thermal and photo-stability [8–12]. Among these, Methylene blue (MB) is a widely used cationic dye known for its persistence and toxicity [13–15]. The presence of MB in water bodies poses severe risks to human health, including potential carcinogenicity and respiratory issues, while also hindering aquatic life by blocking sunlight and reducing dissolved oxygen levels [16–18]. Despite the implementation of various treatment technologies, such as membrane filtration and advanced oxidation, many remain limited by high operational costs and energy demands [19–24] Consequently, adsorption has emerged as a superior and more flexible alternative for MB remediation [25]. Many adsorbent materials have been used in water and wastewater treatment under adsorption techniques. Biochar (BC), a carbon-rich material derived from biomass via pyrolysis, is an especially promising adsorbent due to its cost-effectiveness and environmental compatibility [13,26–28]. Similarly, giant grass (*Cenchrus pedicellatus*), which is indigenous to Ethiopia, is gaining top attention because it is a good precursor material for BC production to be used in water treatment. Pyrolysis at 300-700°C is commonly used to prepare BC under the depolymerization and fragmentation of cellulose, lignin, and hemicellulose. This BC can have a high surface area, low cost, an easily functionalized surface, high porosity, and a stable carbon matrix. However, the actual performance of the BC adsorption depends on pyrolysis temperature, heating duration, preparation conditions, and feedstock. In the context of MB adsorption, maximum BC removal efficiencies of 93.8%, 96.7%, 98.6%, 31.3%, 83.9%, 95.8–

99.4%, 84.1%, 90.3%, 94.2%, 87.6%, 81.1%, 263.2 mg/g, 14.7 mg/g, 318.0 mg/g, 113.4 mg/g, 694.0 mg/g and 212.8 mg/g have been reported [9,29–36]. For these materials, the adsorption removal percentages and the adsorption capacities ranged from 31.3% to 99.4% and 14.7 mg/g to 694.0 mg/g, respectively. However, the scientific community is striving to improve the properties of BC to be an effective and efficient adsorbent for multipollutant removal from actual water and wastewater. These efforts address the fact that pristine biochar often exhibits poor dispersion and a limited capacity to accommodate multiple pollutants simultaneously [37]. Hence, BC modification is essential to enhance its adsorption potential and efficiency.

Among many BC modifications, graphitic carbon nitride (g-C_3N_4) was found to be a good composite to enhance adsorption and photocatalysis processes synergistically [38–40]. Practically, g-C_3N_4 has good thermal and chemical stability and can be distributed on the surface of the BC, which will improve its pollutant removal capacity [8,41]. The nitrogen in the g-C_3N_4 will improve the adsorbent polarity, microstructure, surface functionalities, and surface activity, which enhances the adsorption capacity to interact with the organic compounds, like dyes [42]. However, the application of a magnetic field can be integrated with BC to facilitate the recovery of the spent material. The magnetite surface of the BC can be improved by incorporating magnetite (Fe_3O_4) [43,44]. Exploration of resource recovery on a selective separation basis, Fe_3O_4 is an intrinsically environmentally friendly nanomaterial. This material is a low-cost, thermal-stable, non-toxic separator that generates an efficient external magnetic field that can be used in the water treatment sector. The Fe_3O_4 improves the surface functionalities and external magnetic field of the magnetic BC, which is widely used as an excellent adsorbent in water and wastewater treatment. Fe_3O_4 impregnated with BC helped the adsorbent have good mechanical strength and chemical stability, enabling the spent adsorbent to easily recover. This kind of composite material will upgrade the surface functionalities, magnetic properties, and degradation capacities intentionally to improve dye removal performances. However, there are limited studies that have been conducted under such an intention-experimental condition. Integrating Fe_3O_4 and g-C_3N_4 with BC improves the adsorption inertness of g-C_3N_4, which will significantly enhance its adsorption capacity. This Fe_3O_4-g-C_3N_4-BC composite adsorbent will have improved features like low ecotoxicity, intrinsic external magnetic field, good adsorption capacity, and photocatalyst degradation capacities.

Despite the potential of these individual components, the ternary integration of Fe_3O_4 and g-C_3N_4 onto a sustainable giant grass-derived BC framework remains largely unexplored. The novelty of this work lies in the synergistic coupling of these materials to create a high-performance, magnetically recoverable adsorbent that addresses the specific limitations of

surface inertness and separation difficulty found in conventional BC. Furthermore, the research gap on the giant grass BC- g-C_3N_4 - Fe_3O_4 composite was addressed to reveal the potential of this specific ternary architecture for the high-efficiency treatment of textile industry effluent. Therefore, this study aimed to evaluate the effectiveness of BC-Fe_3O_4-g-C_3N_4 composite for MB removal from aqueous solution using Response Surface Methodology (RSM) and optimizing the interaction between the adsorbent and MB, aiming to reduce the number of experiments and enhance performance. The reusability of the composite was also evaluated to assess its potential for sustainable application in real-world water treatment systems.

2. Materials and Methods

2.1. Chemicals and Reagents

Analytical grade reagents were used throughout this study without further purification. Urea (CH_4N_2O, 99%), sodium nitrate (NaNO3, 99.5%), and ferrous sulfate heptahydrate ($FeSO_4 \cdot 7H_2O$, 99%) were purchased from Sigma-Aldrich for the synthesis of g-C_3N_4 and Fe_3O_4. MB ($C_{16}H_{18}ClN_3S$) was obtained for use as the model pollutant. Sodium hydroxide (NaOH), sulfuric acid (H_2SO_4), and hydrochloric acid (HCl), used for pH adjustment and regeneration, were sourced from Merck. Ethanol (C_2H_5OH, 99.8%) used in the synthesis of the ternary composite, and spectroscopic grade potassium bromide (KBr) used for FTIR analysis, were also obtained from Merck. Deionized water was utilized for all solution preparations and rinsing procedures to ensure the absence of interfering ions.

2.2. Biochar Preparation

The *Cenchrus pedicellatus* sample was gathered on the premises of Addis Ababa Science and Technology University (AASTU) in Addis Ababa, Ethiopia. This sample was cut into small pieces and washed with distilled water. Then, the sample was dried in an oven (Model BOV-T50F) at 105°C for 24 h. Using a muffle furnace, these dried samples were subjected to thermal activation at 600°C for 2 h. At the rate of 5 L/h, an inert atmospheric nitrogen gas was created. This BC was rinsed multiple times with distilled water to produce the adsorbent at a neutral pH. Using a high temperature of 110°C, the wet BC was dried in an oven for 24 h. Finally, the BC was finely ground to 80 µm using a high-speed multi-function miller (Model HC-700), and then stored in an airtight plastic bag until used in the experiment [45].

2.3. Preparation of g-C_3N_4/Fe_3O_4-BC Composite

In many experiments, urea is the most common precursor material for preparing g-C_3N_4. Similarly, in this study, urea was used to synthesize g-C_3N_4 through a thermally induced copolymerization method. About 30 g of urea was placed in a crucible and heated to 550 °C

for 4 h in a muffle furnace at a heating rate of 20°C/min. The material was then cooled, and the pure g-C_3N_4 was collected after being ground into powder for further use [46]. On the other hand, Fe_3O_4 was synthesized by dissolving 2 g of $NaNO_3$ and 3.3 g of $FeSO_4 \cdot 7H_2O$ into 50 mL of distilled water, and the stirring process was conducted for 60 min using the co-precipitation method. Initially, the solution pH was adjusted to 12 using a 1 M NaOH solution. The precipitation formation was enhanced by heating at 80°C and stirring continuously for 5 h. The solution was cooled to room temperature (25°C), and the precipitate was collected by filtration. Then, this semisolid material was washed with distilled water multiple times until a neutral pH was achieved. Finally, the precipitate was dried in an oven at 60°C for 24 h, and the ready-made Fe_3O_4 was placed in an airtight plastic bag [47]. To fabricate the ternary nanocomposite, an equal mass ratio (1:1) of g-C_3N_4) and Fe_3O_4 was first combined. The powders were manually ground in an agate mortar for 20 min to ensure uniform dispersion and intimate contact between the two phases. This binary mixture was then transferred into a beaker containing 50 mL of ethanol and subjected to ultrasonication for 30 min to enhance interfacial interaction. The suspension was dried at 80°C to obtain the g-C_3N_4/Fe_3O_4 nanocomposite. Subsequently, the composite was blended with previously prepared *Cenchrus pedicellatus-derived* biochar at a mass ratio of 2:1 BC to g-C_3N_4/Fe_3O_4. The mixture was again dispersed in ethanol and sonicated for 30 min, followed by oven drying at 80°C for 12 h. The final BC/g-C_3N_4/Fe_3O_4 nanocomposite was ground to a fine powder and stored in airtight containers for subsequent characterization and adsorption experiments. In the end, the composite was prepared by mixing three components of the materials. The specific technique used for the preparation of this composite was the co-precipitation method [48,49]. The details of the preparation process were indicated in Figure 1.

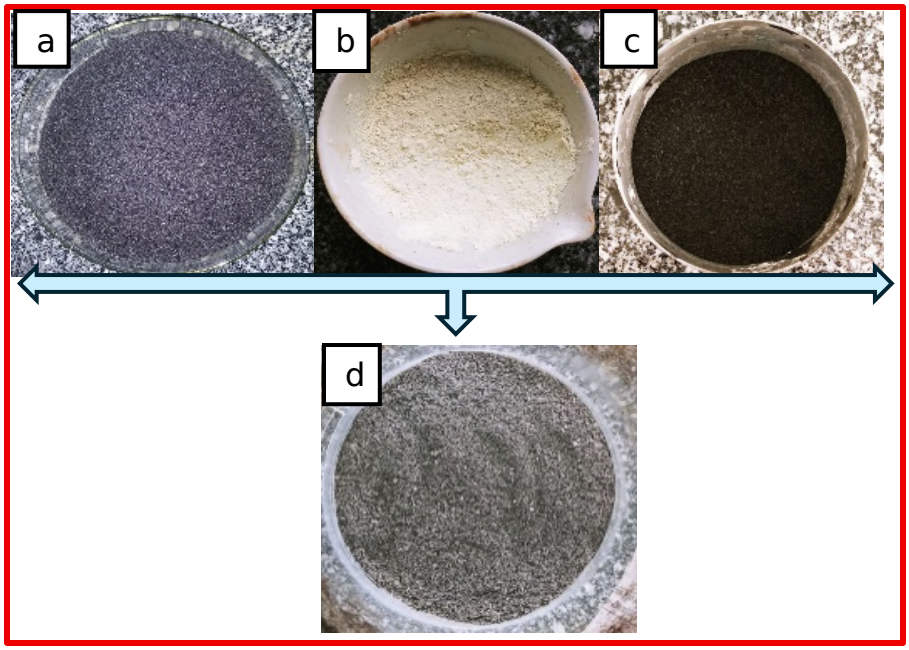

Figure 1. The different processes of nanocomposite preparation; BC (a), g-C_3N_4 (b), Fe_3O_4 (c) composite, g-C_3N_4/ Fe_3O_4| (d)

2.4. Adsorbent Characterization

The content of the composite adsorbent material was assessed using the proximate analysis method. These analyses include determining moisture, volatile matter, ash content, and fixed carbon. The composite evaluation was performed in accordance with the standards set by the American Society for Testing and Materials (ASTM D2866-2869). In this process, Eqs. 1, 2, 3, and 4 are used to determine moisture, volatile matter, ash content, and fixed carbon. Approximately 1g of the adsorbent sample was heated at 105°C for 24 h, 800°C for 8 min, and 550°C for 4 h to determine its moisture, volatile matter, and ash content, respectively.

$$MC = \left(\frac{W_1 - W_2}{W_1}\right) X100 \quad (1)$$

$$VM = \left(\frac{W_1 - W_2}{W_1}\right) X100 \quad (2)$$

$$AC = \left(\frac{W_2}{W_1}\right) X100 \quad (3)$$

$$FC = 100 - (AC + VM + MC) \quad (4)$$

where W_1 refers to the weight of adsorbent before heating/drying (g), W_2 is the weight of adsorbent after ignition (g), AC (%) is the ash content, FC (%) is the fixed carbon, MC (%) is the moisture content, and VM (%) is the volatile ingredient [9].

The surface morphology of the adsorbent was examined using a scanning electron microscope (SEM). Sample preparation and operation were conducted according to the guidelines of the specific machine used. The analysis was performed at 5.00 kV with various resolutions. Each procedure followed the standard operating protocols of SEM (Model FEI Inspect F50, USA). Additionally, the sample SEM characterization was carried out at different resolutions both before and after adsorption. Similarly, Fourier transform infrared (FTIR) was used to determine the functional groups of the adsorbent material. The sample was preprepared by mixing the adsorbent with KBr at a fixed ratio of 2:200. Then, this mixture was ground in a mortar to form a homogeneous mixture. The mixture plate was formed, and FTIR functional scanning was done within the wavelength range of 400-4000 cm^{-1}. Finally, the graph was sketched using data with the help of Origin software version 9.55. Specific surface area of the adsorbent was analyzed using the BET method. The surface analyzer machine, Horiba Model SA-9600, was used. Approximately 0.4 g of the adsorbent sample was subjected to analysis over a period of 2 h at a temperature of 100°C. This experiment was carried out under atmospheric pressure of 700 mmHg using nitrogen gas for both adsorption and desorption processes under the isothermal model of nitrogen. The last characterization technique used in this study was the pH at the point of zero charge (pHpzc), which was determined using the salt addition method. In this method, approximately 0.01 M NaOH and 0.01 M H_2SO_4 solutions were used to adjust the pH of the solution to a range of 2 to 12. At room temperature, the 0.5 g adsorbent solution in the flask was set to be mixed at a mixing speed of 150 rpm for 36 h, which was agitated using an orbital shaker (Model 2346-1CEQ). Then, the change in pH (pHf-pHi) was calculated. A graph plotting initial pH against change in pH was constructed to ascertain the pHpzc at the X-intercept [50–52].

2.5. Optimization of MB Removal

The stock solution of the dye was prepared by adding 1 g of MB to a 1000 mL volumetric flask and filling it with distilled water up to the 1 L mark. Subsequently, the dissolution process was executed under agitation using a magnetic stirrer at a mixing speed of 125 rpm, and an MB concentration of 1000 mg/L was achieved. With the principle of dilution, the required MB solution of 100 and 150 mg/L was prepared, as indicated in Table 1. With these concentrations, the adsorption process was carried out under specific experimental conditions, which were further agitated using an orbital shaker at 125 rpm and then filtered via Whatman filter paper. The concentration of the dye was analyzed using a UV–Visible spectrophotometer at a wavelength of 668 nm [53]. The removal efficiency was calculated using Eq. 5.

$$R\% = \left(\frac{C_1 - C_f}{C_f}\right) X100 \quad (5)$$

where R% is the MB removal percentage, C_i (mg/L) and C_f (mg/L) are the initial and final MB concentrations after adsorption treatment

Table 1. Adsorption factors and their levels under the experimental design matrix for input variables

Factor	**max**	**min**
pH	3	11
Adsorbent Dose (g/100 mL)	0.5	2
Initial MB concentration (mg/L)	100	150
Contact Time (min)	45	100

This adsorption study was conducted under a factorial experimental design of four with two levels, resulting in several adsorption runs. This used Face center alpha Design Expert software (Version 13), Response surface methodology (RSM)-Central composite design (CCD). Under experimental design, the number of experiments was calculated using Eq. 6.

$$N = 2^F + 2F + X0 \quad (6)$$

where N represents experimental runs for adsorption treatment, the number of experimental runs, F is the number of factors in the experiment, and X0 refers to the central point with the number of replicates

Based on this analysis of coding to the RSM of CCD, in these experimental runs, all batch experiments were 30, which is designated by N under consideration of the number of factors in the experiment, and the replication of the central points is 4 and 6, respectively. These were calculated as factorial points, 2^4 is 16, and axial points, 2×4 is 8, and center points, 6. The regression analysis was performed under a quadratic regression model established by response surface methodology under CCD using Eq. 7.

$$Y = \beta o + \sum_{i=1}^{n} \beta i Xi + \sum_{i=1}^{n} \beta ii Xi^2 + \sum_{i=1}^{n} \sum_{j=i+1}^{n} \beta ij Xi Xj + \varepsilon \quad (7)$$

where Y is the predicted response which is the removal efficiency of MB, $\beta 0$ is the intercept term, βi is the linear coefficients for each factor, βii is the quadratic coefficients for each factor, βij is the interaction coefficients between factors, Xi, Xj is the coded independent variables (pH, dose, concentration, and time), ε is the Random error term and n represents the number of independent variables or factors

2.6. Adsorption Isotherm and Kinetics

The equilibrium relationship between the adsorbent and the pollutant was evaluated using various isothermal models. In this study, initial MB concentrations ranging from 100 to 150 mg/L were utilized, while the pH, adsorbent dose, and contact time were maintained at 7.0, 1.25 g/100 mL, and 72.5 min, respectively. All solutions were agitated using an orbital shaker at a constant speed of 125 rpm. The linearized forms of the Langmuir, Freundlich, and Temkin models were employed to determine whether the adsorption occurred via monolayer or multilayer formation. While the Langmuir and Freundlich models address surface coverage, the Temkin model specifically accounts for adsorbent–adsorbate interactions, assuming a heterogeneous surface where the heat of adsorption decreases linearly with coverage. The fundamental parameters for the Langmuir, Freundlich, Temkin, and Dubinin-Radushkevich isotherms were calculated using Eqs. 8, 10, 11, and 12, respectively, while the Langmuir-based separation factor (R_L) was determined via Eq. 9. To assess the influence of residence time, contact times were varied from 45 to 100 min, with other parameters fixed at an initial MB concentration of 125 mg/L, pH 7.0, and a dosage of 1.25 g/100 mL at 125 rpm. The removal rate as a function of time was estimated using linear adsorption kinetics. These processes were modeled using pseudo-first-order, pseudo-second order, and intraparticle diffusion equations (Eqs. 14–16), consistent with established literature [54–57].

$$\frac{Ce}{qe} + \frac{1}{qmax}\ Ce + \frac{1}{KL\ qmax} \quad (8)$$

$$RL = \left(\frac{1}{1 + (KL * Ci)}\right) (9)$$

$$Log\ qe = Log\ KF + \frac{1}{n} LogCe (10)$$

$$qe = \frac{RT}{BT} lnAT + \frac{RT}{BT} lnCe$$

$$lnqe = lnqDRmax - \beta\epsilon^2 \quad (12)$$

$$\epsilon = R * T * \ln\left(1 + \left(\frac{1}{Ce}\right)\right)$$

(13)

$$\log(q_e - q_t) = \log q_e - \frac{K_{1t}}{2.303} \quad (14)$$

$$\left(\frac{t}{q_t}\right) = \frac{1}{k_2 * (q_e)^2} + \left(\frac{t}{q_e}\right) \quad (15)$$

$$\text{Log qt} = \text{Log Kp} + \frac{1}{n}\text{Log (t)} \quad (16)$$

Where KL (L/mg) refers to the Langmuir constant, q_{max} (mg/g) is the maximum monolayer adsorption capacity of the adsorbent, KF denotes adsorption capacity (mg/g), and 1/n denotes as adsorption intensity, q_e (mg/g), is the mass of adsorbed material at equilibrium, q_t (mg/g) is the mass of pollutant adsorbed at time t, BT is a Temkin constant based on the heat of adsorption, R is the universal gas constant, T is the temperature of the system, AT equilibrium binding constant, K_1 is the Pseudo-first-order constant (1/min), K_2 is the Pseudo-second-order constant (g/mg/min), and K_p is the constant value (mg/g/min$^{0.5}$), lnq($_{D\text{-}Rmax}$)(mg/g) denotes the theoretical maximum adsorption capacity, while β (mol^2 k/J^2) denotes the Dubinin-Radushkevich constant. The term ϵ denotes the Polanyi potential, R denotes the universal gas constant (8.31 J/mol K), and T (K) denotes the absolute temperature.

2.7. Regeneration Study

Adsorbent regenerating and reuse are one of the main components of efforts to secure environmental sustainability. Adsorbent reusability is ideal, cost-effective, and environmentally sustainable, which is based on the principle of replacing the utility of fresh materials. Adsorption and desorption of the composite adsorbent were done using a 1 M NaOH solution [49,58]. The experimental condition was set as an initial MB 300 mg/L in 250 mL Erlenmeyer flasks, pH level of 7, composite adsorbent 3 g, and the experiment was maintained at a temperature of 25°C. Each experiment was performed using Erlenmeyer flasks containing 100 mL of working solution, subjected to agitation at 400 rpm for a duration of 120 min, employing a magnetic stirrer. Upon completion of the experimental adsorption and desorption process, the concentration of MB within the filtrates was determined using a UV-Spectrophotometer. Finally, the desorption efficiency of the materials after reuse was calculated.

3. Results and Discussion

3.1. Adsorbent Characteristics

3.1.1. Proximate Analysis

In determining the properties of our adsorbent material, proximate analysis is one of the methods that can be used. Importantly, the amount of fixed carbon and ash content is crucial for predicting proper interaction between the adsorbent and incoming pollutants in the aqueous solution. Fixed carbon is basically nonvolatile carbon, whereas the ash content is the inorganic material that remains after heating the adsorbent at high temperature for a specific time. The details and the percentage of proximate analysis of the adsorbent are given in Table 2. The amount of fixed carbon found in this study was 55.06%, indicating that a higher content of fixed carbon is a desirable characteristic of a good carbonaceous adsorbent for the physisorption process. From the fixed carbon value perspective, the adsorbent has a high possibility of having a high surface area and adsorption capacity to purify and remediate water and wastewater. However, to have concrete conclusions, the study of surface chemistry (functional groups) and the BET specific surface areas should be conducted. Similarly, the ash content of the adsorbent was determined, and a significantly small percentage (4.02%) was found. The low ash content is a good indicator of the carbonaceous adsorbent. This is a good indicator of a good adsorbent since there is a possibility that the inorganic minerals might cover and block the volumes and the active sites of the adsorbent surface. This value is still higher compared to other BC or active carbon originating from biomass. The value might be partially attributed to the iron oxide that was used in the preparation of the composite adsorbent. The proximal analysis of the current adsorbent shows less than 10% of ash content and greater than 50% of fixed carbon, which is in a promising adsorbent category [9,59].

Table 2. The adsorbent proximate analyses and the composition percentages are presented

Proximate Analysis Parameters	**Value in %**
Moisture Content (%)	7.62
Volatile Matter (%)	33.3
Ash Content (%)	4.02

Fixed Carbon (%)	55.06

3.1.2. SEM analysis

The surface morphology of the ternary composite was investigated via SEM to elucidate the structural changes occurring during the removal process. Figure 2a-b presents the SEM micrographs of the adsorbent before and after MB adsorption, respectively. Before adsorption (Figure 2a), the composite surface exhibits a highly heterogeneous and cavernous structure characterized by an extensive network of open macropores and micro-cracks. These features are derived from the structural integrity of the giant grass BC framework. High-magnification images reveal the successful decoration of the BC flakes with Fe_3O_4 and g-C_3N_4 particles, which appear as irregular clusters that increase the overall surface roughness and active site density. This rough, non-uniform topography is a critical precondition for facilitating the diffusion of dye molecules into the inner pore channels. Following the adsorption treatment (Figure 2b), a dramatic change in surface morphology is evident. The previously sharp edges and deep pore cavities appear significantly smoothed and "clogged," indicating the successful accumulation of MB molecules across the adsorbent surface. The distinction between the composite particles becomes less defined as the MB dye forms a molecular layer that fills the pores and coats the g-C_3N_4/Fe_3O_4 active sites. This transition from a highly porous, jagged structure to a relatively "saturated" and flatter surface morphology confirms that the removal process is largely driven by pore-filling mechanisms and strong surface interactions, which are well-aligned with the high removal efficiencies reported in the optimization study. This structural evidence is further corroborated by the reduction in surface area and pore volume typically observed in BET analysis following dye loading.

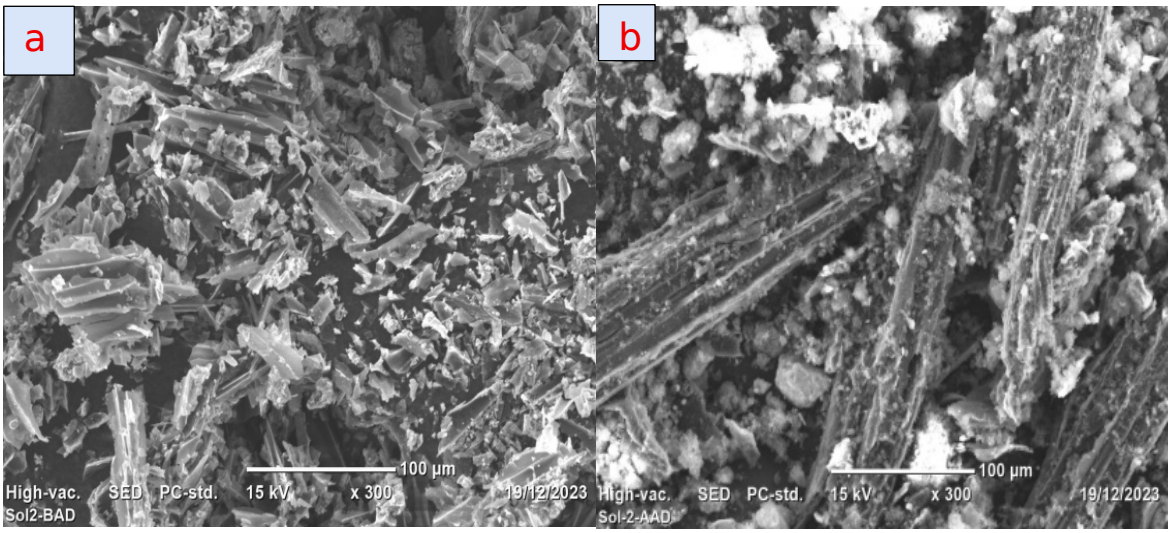

Figure 2. The SEM analysis of the composite adsorbent before adsorption (a) and after the treatment (b)

3.1.3. BET analysis

The specific surface of the composite adsorbent was determined before and after adsorption using the BET method under N_2 adsorption/desorption process. The specific surface area of the composite adsorbent before and after adsorption was found to be 690 and 410.21 g/m^2. Unfortunately, the external surface area, pore volume, and diameter were not determined in this study. After removal of the MB via adsorption, the specific surface area of the adsorbent was significantly decreased to 410.21 g/m^{-2}, which is directly proportional to the amount of the MB attached to the active sites of the adsorbent. The high value of the specific surface area showed that the adsorbent has a huge potential and competent candidate for the removal of pollutants from water and waste aqueous solutions. Moreover, this property also aligned with the surface morphology analysis and the percentage of the fixed carbon. However, to understand the complete properties of the adsorbent, water chemistry in the reaction media and the surface functionalities of the adsorbent are essential. In general, high value of the specific surface area of this adsorbent is high and higher than many values reported in the literature [50].

3.1.4. The pHpzc

The pHpzc value of the composite adsorbent was analyzed, and the corresponding findings are shown in Figure 3. The net zero charge on the surface of the adsorbent was found to be 8.2. This implies that the number of positive and negative charges is equal. The properties of this adsorbent surface enhance interaction with the positively charged adsorbent by more than 8.2 units of pH, whereas the negatively charged pollutants will be synergistically helped to be removed at pH levels less than 8.2 units. On the other hand, MB is a cationic dye that will be favored in the negatively charged adsorbent surface. Irrespective of considering the other factors in the removal of the MB in the adsorption process, MB can be effectively removed from the solution when the pH is above 8.2 units. Normally, the pHpzc value of the different adsorbents can be found at different pH values. However, adsorbent surface chemistry and interaction with water chemistry are essential to find an efficient adsorption process.

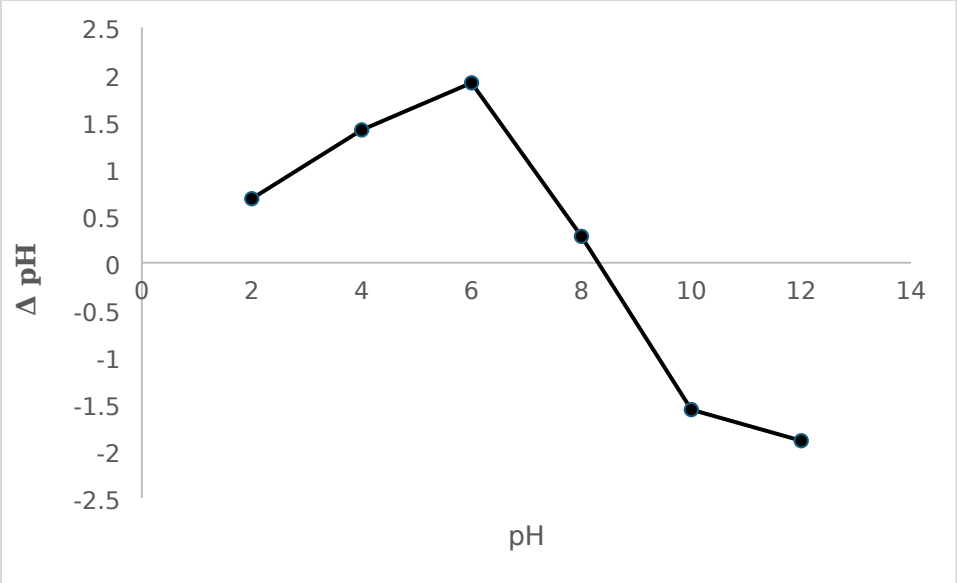

Figure 3. The pHpzc of the composite adsorbent

3.1.5. FTIR Analysis

The FTIR analysis of the composite adsorbent was conducted, and some functional groups were identified and shown in Figure 4. There are about 8 clearly observable peaks that have been discovered. These peaks are found to be at 569, 806, 879, 1238, 1315, 1407, 1564, 1619, 1741, and 3176 cm^{-1}**.** Among all the most important peaks for these discussions, 806, 1238, 1407, 1564, and 3176 are C=C bending vibrations of an alkyl aryl ether, indicating the presence of a carboxylate ion ($R\text{-}COO^{-}$), amide conjugated carbonyl group stretching with N-H bend and C-N stretch, and O-H stretching of an alcohol with a weakly broadened peak, respectively. In many of those functional groups, the lower intensity of the peaks was observed, which might be attributed to the insignificant presence of those functional groups in the adsorbent sample. The evaluation of the presence of the functional groups before and after adsorption, the shifting or the disappearance of the peaks was not observed. The only prominent finding in this analysis is the diminishing of the peaks. However, the presence of many functional groups is a promising feature for this adsorbent to be effective in the removal of the multi-pollutants in complex wastewater matrices. This is the only possible scenario, but sometimes other factors are more dominant, and the removal performance might be minimal or ineffective. In this study, there is the possibility that the composite adsorbent will work effectively in the wastewater treatment sector from the functional group's point of view.

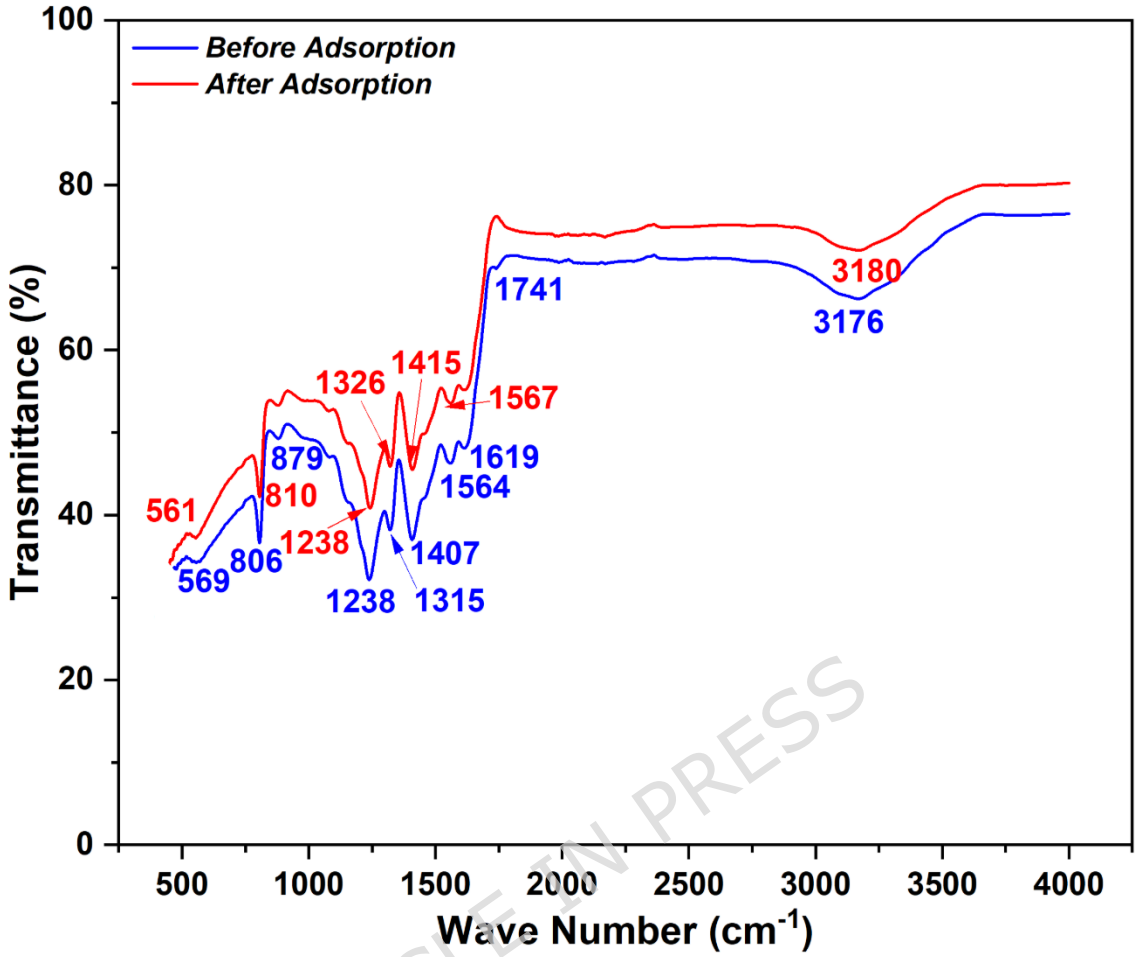

Figure 4. The FTIR graph of the composite adsorbent

3.2. Optimization of MB removal

The removal of MB was evaluated under specific experimental conditions to identify the optimal parameters for maximum efficiency. As detailed in

Table 3, the removal efficiency ranged from 71.2% to 93.3%, with the optimum performance of 93.3% occurring at an initial MB concentration of 100 mg L^{-1}, pH 7, 1.25 g/100 mL dose, and 72.5 min. The minimum removal (71.2%) observed at pH 3 and low contact time confirms the significant influence of surface protonation. The influence of individual factors is profound; specifically, the solution pH and adsorbent dose act as the primary drivers of the adsorption mechanism. Below the pHpzc of 8.09, the densely positively charged surface limits the approach of the cationic MB molecules, making pH a dominant factor in controlling removal percentages. Furthermore, the prominence of these individual influences over secondary interactions is consistent with recent findings in composite adsorbent

optimization, where the intrinsic surface properties of the BC-based material dictate the overall removal kinetics [58].

Table 3. Optimization of MB adsorption with the specific removal factors at specified levels

Run	pH	Adsorbent dose (mg/100 mL)	Initial MB concentration (mg/L)	Contact time (min)	Removal Efficiency (%)
1	3	0.5	150	100	75.83
2	7	1.25	125	72.5	87.91
3	3	0.5	150	45	71.85
4	3	0.5	100	45	73.98
5	7	1.25	125	72.5	85.65
6	11	1.25	125	72.5	79.56
7	3	1.25	125	72.5	79.01
8	11	0.5	100	45	76.81
9	7	1.25	125	72.5	86.11
10	7	1.25	125	45	77.42
11	7	1.25	125	72.5	85.65
12	11	0.5	100	100	82.21
13	7	1.25	150	72.5	92.23
14	11	0.5	150	100	82.42
15	3	2	100	100	81.64
16	3	2	150	45	80.11
17	7	1.25	125	72.5	85.38
18	7	1.25	125	72.5	86.14
19	11	2	150	45	80.54
20	7	1.25	100	72.5	93.25
21	7	0.5	125	72.5	78.52
22	3	0.5	100	100	71.21
23	11	2	100	45	82.54
24	11	2	150	100	81.52
25	7	1.25	125	100	78.61
26	3	2	150	100	77.58
27	11	2	100	100	83.21
28	3	2	100	45	83.43
29	7	2	125	72.5	80.42
30	11	0.5	150	45	77.12

3.3. The regression analysis and ANOVA of MB removal

The quadratic model was employed to quantify the influence of individual effects and their interactions. As shown in Table 4, the model F-value of 19.02 and a p-value < 0.0001 confirm that the regression model is highly significant. The R^2 value of 0.90 indicates that 90% of the variability in MB removal is accounted for by the identified factors. The analysis reveals that the main effects of pH (A) and adsorbent dose (B), along with their quadratic terms (A^2, B^2,

C^2, D^2), exert a more substantial influence on the system than the interaction terms alone. Following the methodology suggested by recent literature, the hierrchy of factor influence was determined to be driven heavily by the quadratic effects, which indicates a non-linear relationship between the factors and the removal efficiency. This suggests that there is an optimum range for each factor beyond which the incremental benefit to adsorption diminishes. Specifically, the high significance of A and B proves that the surface chemistry and site availability are the most critical individual influences in this aqueous system. While interactions like AB (pH and dose) and AD (pH and time) are present, the individual impact of each factor provides the necessary signal to describe the treatment process accurately, ensuring the model's predictive reliability for high-impact applications [60]. The empirical relationship between the target response and the process variables is quantitatively expressed through the second-order polynomial regression model as shown in Eq. 17.

$$\text{MB Removal \%} = 85.05 + 1.74A + 2.28B - 1.29AB + 0.96AD - 0.91BD - 4.67A^2 - 4.48B^2 + 8.79C^2 \cdot 5.94D^2 \quad (17)$$

where A represents the solution pH, B is the adsorbent dose, C is the initial MB concentration, and D is the contact time.

In this analysis, the degree of the impact can be described as decreasing in order of the main and interaction effects, $C^2 > D^2 > A^2 > B^2 > B > A > AB > AD > BD$. It is also easy to understand that some factors and interactions negatively influence the removal of the dye. In these phenomena, interaction between the pH and the adsorbent dose, the adsorbent dose and contact time, and the interactions of individual factors among themselves, including the pH solution, adsorbent dose, and contact time, are clearly observed. The remaining model terms, like solution pH, the adsorbent dose, and the interactions between the solution pH and contact time, and adsorbent dose and contact time, and initial MB concentration with itself, enhanced the adsorption of the dye. The regression model's goodness of fit can be evaluated from the coefficient of determination and the adjusted coefficient of determination. Under these circumstances, the R^2 of 0.90 and adjusted R^2 of 0.75 were found. This indicated that the removal of the MB dye was described by the regression model with about 90% in this analysis, and only about 10% variation, which is incapable of describing the treatment of the MB removal process. It was indicated that the model is adequate, with good precision measures, which indicates an adequate signal. Similarly, the Model F-value of 19.02 implies that the regression model is significant in general. However, the noise might cause only a 0.01% chance that an F-value is larger than what is supposed to be. In general, the regression

model is well fitted with the experimental data, and the variation of the treatment was adequately described by the model.

Table 4. Analysis of variance (ANOVA) for the quadratic model describing the effects of pH (A), adsorbent dose (B), initial methylene blue (MB) concentration (C), and contact time (D) on the response

Sources	Source of square	df	Mean square	F value	P value	
Model	744.17	14	53.15	19.02	< 0.0001	significant
A-pH	54.39	1	54.39	19.47	0.0005	
B-Adsorbent dose	93.57	1	93.57	33.49	< 0.0001	
C-Initial MB concentration	4.58	1	4.58	1.64	0.2199	
D-Time	6.04	1	6.04	2.16	0.1621	
AB	26.63	1	26.63	9.53	0.0075	
AC	0.1849	1	0.1849	0.0662	0.8005	
AD	14.94	1	14.94	5.35	0.0354	
BC	12.39	1	12.39	4.43	0.0525	
BD	13.29	1	13.29	4.75	0.0456	
CD	2.42	1	2.42	0.8653	0.3670	
A^2	56.50	1	56.50	20.22	0.0004	
B^2	52.11	1	52.11	18.65	0.0006	
C^2	199.97	1	199.97	71.56	< 0.0001	
D^2	91.41	1	91.41	32.71	< 0.0001	
Residual	41.92	15	2.79			
Lack of Fit	37.72	10	3.77	4.50	0.0553	not significant
Pure Error	4.19	5	0.8383			
Cor Total	786.08	29				

The adequacy and fitness of the quadratic model were further validated through several diagnostic statistical measures Table 5. The R^2 value of 0.9467 indicates that the model can account for approximately 94.7% of the total variation in MB removal, demonstrating a high

degree of correlation between the experimental and predicted values. The small difference between the Adjusted R^2 (0.8969) and Predicted R^2 (0.7549) confirms that the model is not over-fitted and possesses strong predictive capability. Furthermore, the low Coefficient of Variation (C.V.%) of 2.06% reflects the high precision and excellent reliability of the experimental runs. Most importantly, the 'Adequate Precision' value of 18.2333, which significantly exceeds the threshold of 4, indicates a high signal-to-noise ratio. This confirms that the model can be used to navigate the design space effectively, ensuring that the optimization of the ternary BC composite is statistically robust and reproducible.

Table 5. Statistical fit summary and diagnostic measures for the MB removal model

Statistical Parameter	**Value**
Standard Deviation	1.67
Mean	81.26
Coefficient of Determination (R^2)	0.9467
Adjusted R^2	0.8969
Predicted R^2	0.7549
Coefficient of Variation (C.V. %)	2.06
Adequate Precision	18.2333

The statistical adequacy and predictive accuracy of the developed quadratic model were rigorously validated through diagnostic plots, as presented in Figure 5. The normal probability plot of residuals (Figure 5a) exhibits a linear trend, indicating that the experimental errors are normally distributed and that the model assumptions are satisfied. Furthermore, the correlation between the predicted and the actual experimental data (Figure 5b) shows that the data points are clustered along the 45° diagonal line. This degree of alignment, supported by the R^2 value of 0.9467, confirms that the model can accurately predict the MB removal efficiency across the investigated experimental design space.

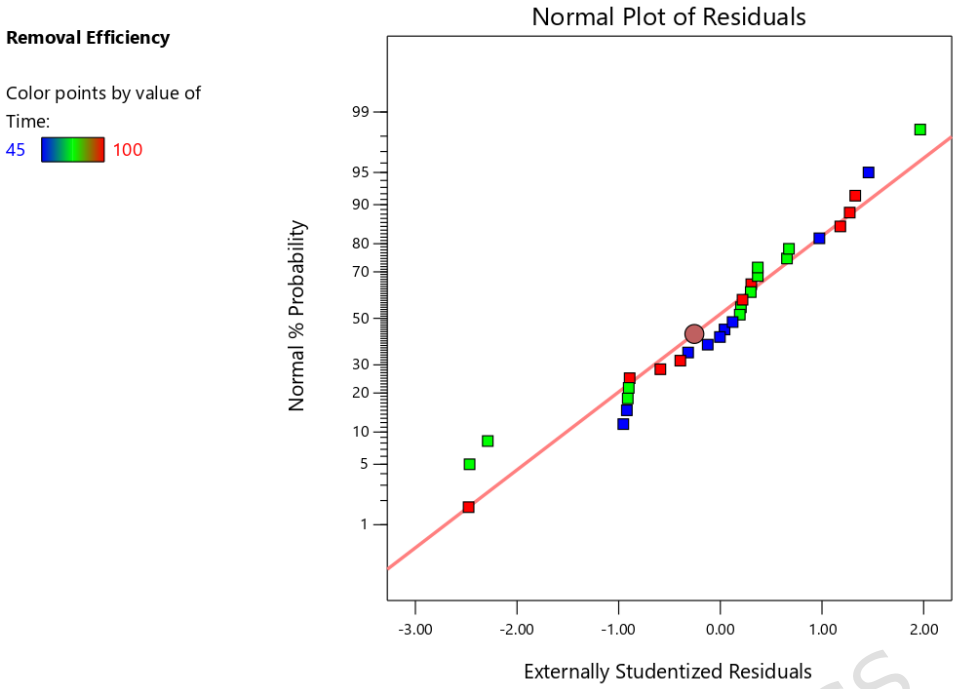

A

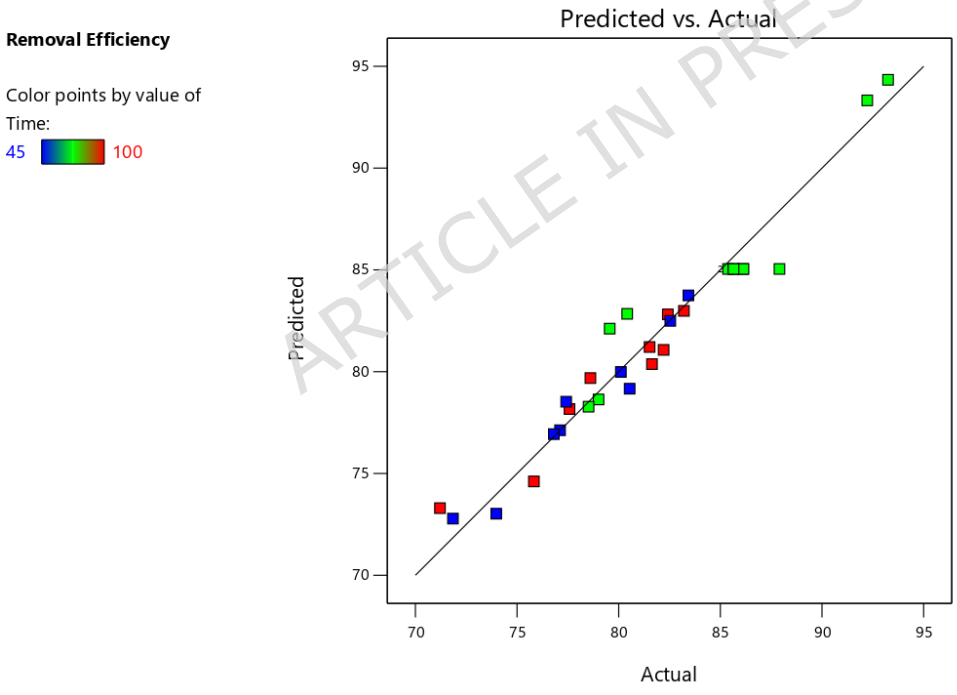

B

Figure 5. Statistical diagnostic plots for the MB removal model: (a) Normal plot of residuals, and (b) Predicted versus actual experimental data

3.4. The Interaction Effects of Factors on MB Adsorption

3.4.1. The interaction of pH and Adsorbent dose

In the study of the interaction effect, the removal of the MB does not only depend on the value of the individual factors. The interactions between factors are equally important in some situations. Based on the quadratic regression model, several of the interactions are found to be insignificant in influencing the remediation of the MB. Hence, the interaction of AB and AD is the only significant interaction under the actual values of C and D. This interaction effect occurred between the pH and the adsorbent dose, which are inversely impacted on the removal of the MB, as indicated in Figure 6. This pattern was also confirmed under the analysis of the quadratic regression model. However, the individual value of the factor might indicate that the removal of MB can be increased by increasing the value of the adsorption factor or vice versa. Practically, the most important element in the adsorption process is the interaction effect, which can be observed. The maximum projected removal of the MB was found under the solution pH and adsorbent dose, which was depicted in a 3D pictorial representation (Figure 6).

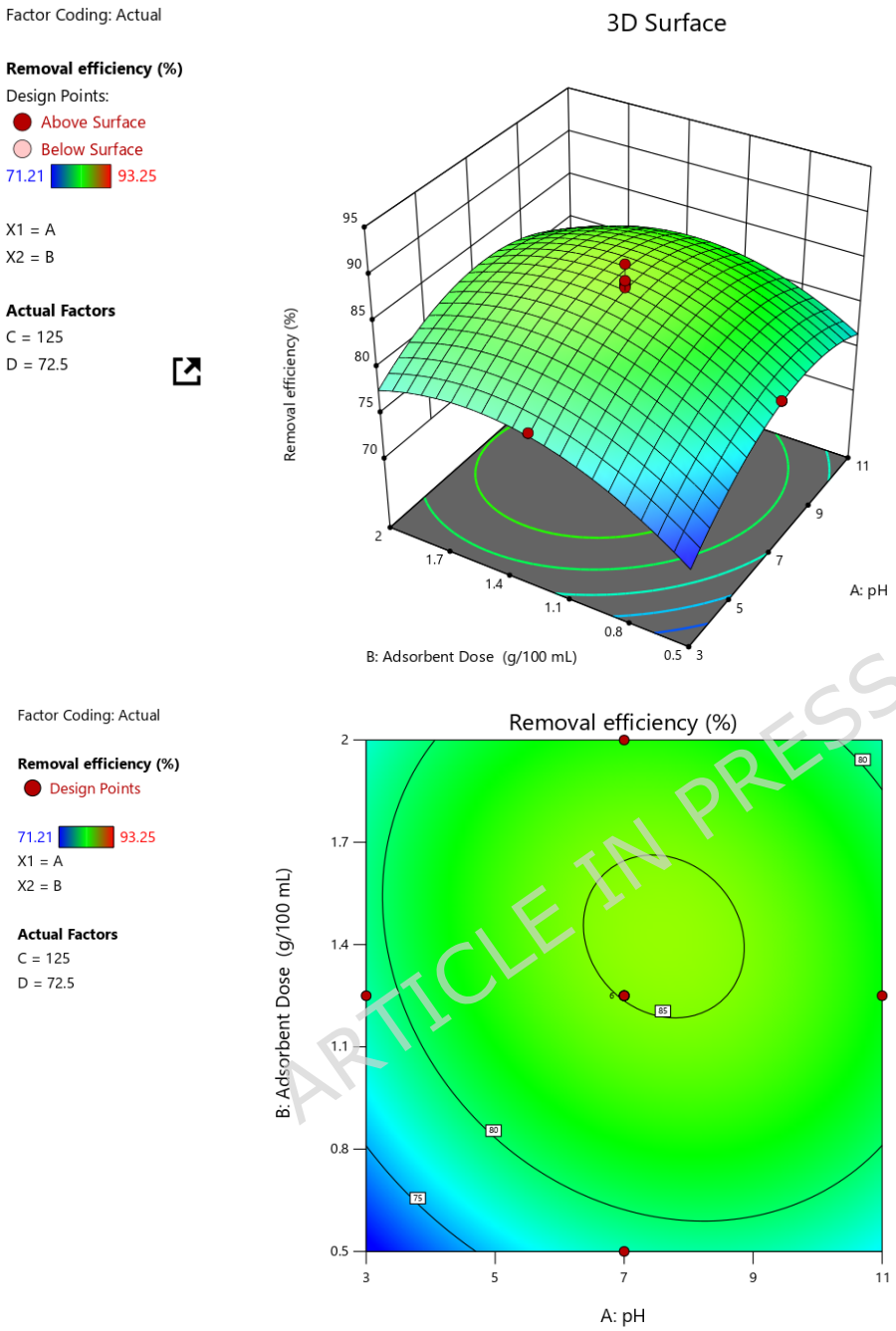

Figure 6. The interaction effect of the influence of solution pH and adsorbent dose on the prediction of MB removal.

3.4.2. The interaction of pH and Contact time

The second most important interaction is the one between the solution and the contact time. This interaction was performed using the RSM under the constant values of the initial MB concentration and adsorbent dose. This interaction effect was demonstrated in a 3D pictorial

representation, indicating that it was positively influencing the removal of the MB from the aqueous solution. The maximum removal of MB from the aqueous solution was depicted on contour form and a three-dimensional plot of the response surface, as indicated in Figure 7. However, the evaluation of the individual factor indicated that the solution pH is positively enhanced in the adsorption of the dye, whereas the contact time is unfortunately insignificant at all. The overall analysis indicates that the predicted value is in line with the actual adsorption experimental value, which implies the model's fitness.

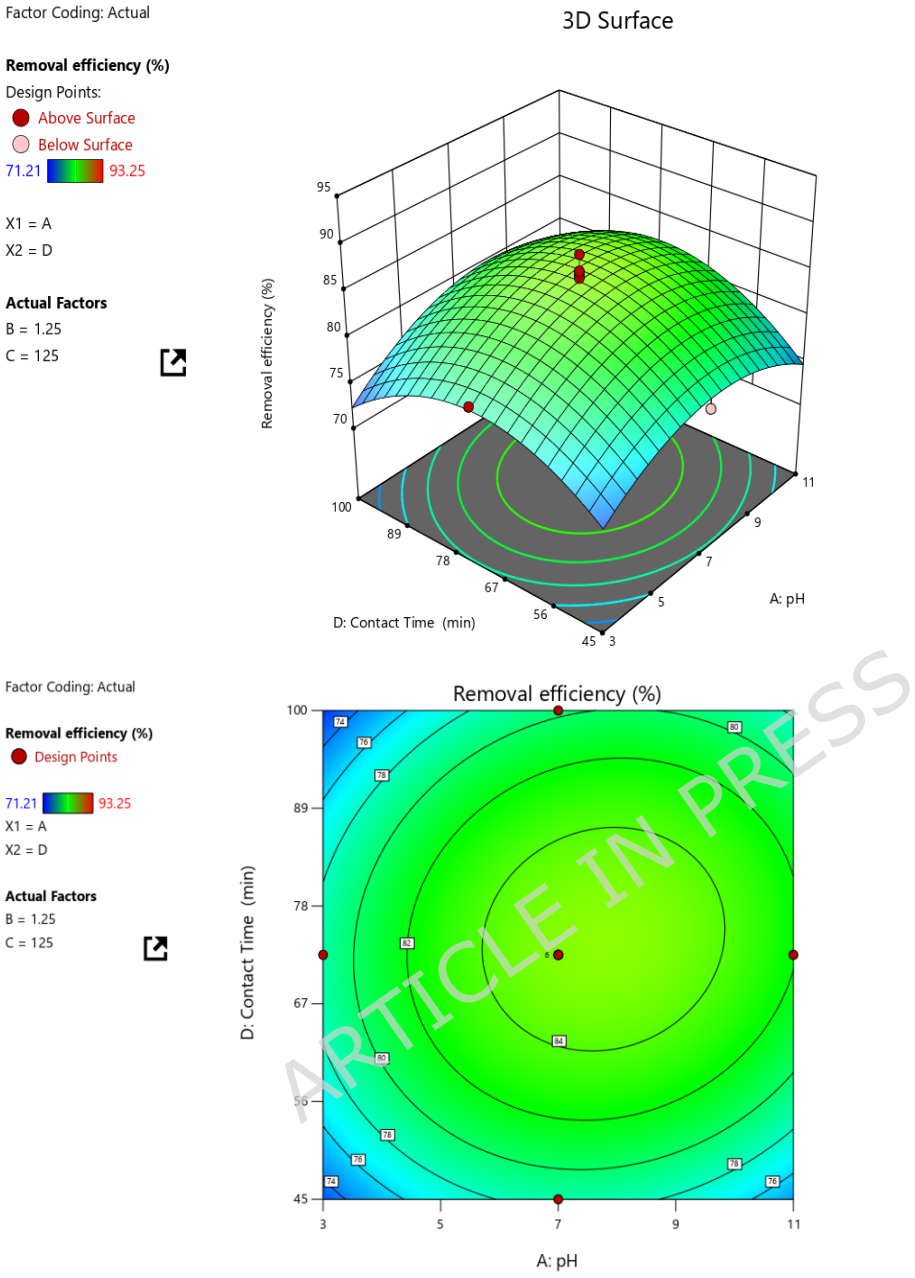

Figure 7. The interaction effect of the influence of solution pH and contact time on the prediction of MB removal

3.5. Adsorption Isotherms

The adsorption isotherms of the MB removal were investigated under different MB concentrations using fixed values of the solution pH, adsorbent dose, and contact time. Based on the data, the evaluation of the four isotherm models was done using the linearized form of the equation for each model. The details of the outcomes are presented in Table 6. The adsorption of the Freundlich, Langmuir, Temkin, and Dubinin-Radushkevich was determined

based on the dye removal under specific experimental conditions. Consequently, the experimental data best fit with the Langmuir model at an R^2 value of 0.99. This value is maximum among the four models, and close to which implies a better fit with reality. Basically, the Langmuir model is based on two assumptions, which are the single-layer adsorption and a uniform surface with equal binding energy. According to this model, the adsorption mechanism of the MB removal aqueous solution is homogeneous and uniform with a single layer on the surface of the adsorbent. The dimensionless separation factor (R_L) confirmed the favorability of the adsorption process across all studied conditions. Specifically, at the maximum initial concentration of 150 mg/L, the R_L value was found to be 0.342. Since this value falls within the established range of $0 < R_L < 1$, it indicates that the adsorption of MB onto the composite is highly favorable. Furthermore, the Freundlich constant (n) was determined to be 4.227. Because n lies between 1 and 10, it provides additional evidence of a favorable adsorption intensity and a strong affinity between the adsorbent surface and the MB molecules. Moreover, it is assumed that the vacant sites are also of a similar shape and provide an equal opportunity for the adsorbent to interact with the adsorbate under the same binding energy throughout the treatment process. However, practically, it is difficult to experience the same situation using adsorbents for water and wastewater treatment. There is a high possibility that this kind of adsorption mechanism is experiencing a chemical adsorption process. This is mainly attributed to the repulsion phenomenon to make a double layer.

Table 6. The adsorption isotherms details and the values of the parameters for different models

Isotherm models		
Langmuir	R^2	0.9934
	q_{max} (mg/g)	1250
	K_L (L/mg)	0.0128
	Equation	0.0008X+0.0621
Freundlich	R^2	0.7886
	N	4.227
	K_f ((mg/g) $(L/mg)^{1/n}$)	10.783
	Equation	0.2366X+2.378
Temkin	R^2	0.8832
	b (J/mol)	0.047
	Kt (L/g)	0.625
	Equation	Y=472.31X-223.68
	R^2	0.7416

Dubinin-Radushkevich	qDRmax (mg/g)	3.0356
	β (mol^2 k/J^2)	0.0012
	Equation	Y= -0.0012X+3.0356

3.6. Adsorption kinetics and intraparticle diffusion

In the adsorption process, how fast the adsorbate attaches to the surface of the adsorbent was studied using the adsorption kinetics. The adsorption kinetics were carried out, and the obtained data were operated under the kinetics model, and the findings are presented in Table 7. This kinetics study was evaluated using the intraparticle diffusion model, pseudo-first order, and pseudo-second order. In the physicochemical interaction of adsorbate and adsorbent, the rate-determining step was determined. The adsorption experimental data were fitted with the intraparticle diffusion model, pseudo-first order, and pseudo-second order, and the R^2, q_e experimental, and q_e were calculated. Based on those factors, the experimental data were more described by pseudo-second-order kinetics at R^2 0.86. This model implies that the rate of adsorption was based on the adsorption capacity rather than other factors like pollutant concentration. Generally, this kinetic study is helpful to determine the rate of the removal of the MB from the aqueous solution under the composite adsorbent.

Table 7. The study of MB adsorption kinetics and the corresponding kinetics model values

Kinetics model	**Kinetic parameters**	**Values**
Pseudo-first-order	R^2	0.5540
	qe (mg/g)	2.077
	K_1 (1/min)	0.0035
	Equation	Y=0.0152X+0.7311
Pseudo-second-order	R^2	0.8565
	qe (mg/g)	277.778
	K_2 (g/mg min)	0.00082
	Equation	Y=0.0036X-0.0632
Intraparticle diffusion	R^2	0.7024
	C	669.31
	K_{ID} ((mg/g) min$^{0.5}$)	28.214
	Equation	-28.214X+669.31

The comparative performance of the synthesized ternary composite against various biochar-based and metal-oxide nanocomposites reported in recent literature is summarized in Table 8.

Table 8. Comparative assessment of MB adsorption performance and optimized operational parameters between the current ternary composite and previously reported adsorbents.

Precursor material	**pH**	**Initial Concentration (mg/L)**	**Contact time (min)**	**Adsorbent dose (g/L)**	**MB Removal (%)**	**References**
BC/Fe_3O_4 nanocomposite	9	100	40	0.4	99.99	[61]
BC/$NaC_6H_7O_6/(CH_2CH)_n$ nanocomposite	8	100	180	0.5	96.51	[62]
$MnFe_2O_4$/BC nanocomposite	5	15	20	0.7	95.00	[63]
Polyamide-Vermiculite Nanocomposites	5	15	60	0.15	99.00	[64]
SNF/MNP/PS nanocomposite	6	100	90	0.3	82.70	[65]
BC/GO/Fe_3O_4 nanocomposite	9	25	85	3	99.00	[58]
BC/ZnO nanocomposite	-	160	225	1	95.19	[66]
$CuMn_2O_4$/chitosan micro/nanocomposite	6.5	1	5	1.25	98.98	[67]
BC/Ag nanocomposite	-	25	75	5	88.40	[68]
Biochar-Fe_3O_4-g-C_3N_4 composite	7	100	72.5	12.5	93.3	This study

3.7. Regeneration Study

Evaluation of the adsorbent material in terms of reusability is essential in addition to the adsorption capacity. The composite adsorbent's recyclability and reusability were studied over seven cycles, and the adsorption performance is presented in Figure 8. The optimum reusability of the adsorbent was determined under the adsorption and desorption processes of the MB under optimal adsorption conditions. In the process of checking the reusability of the adsorbent, the adsorption performance of the material ranged from 78.2 to 12.2%. The

difference in the removal of MB between the first and the seventh cycle is 66%. This implies that the performance of the adsorbent materials sharply decreased from one cycle to another. Therefore, it is very important to understand that the reusability of the composite adsorbent will never go beyond the first three cycles. Even though the composite adsorbent was effective in the removal of the MB from aqueous solutions, the reusability of the material is not effective under the current study approach. In conclusion, the recycling of this material required further improvement, which might require another method to be used for practical water treatment at an industrial level.

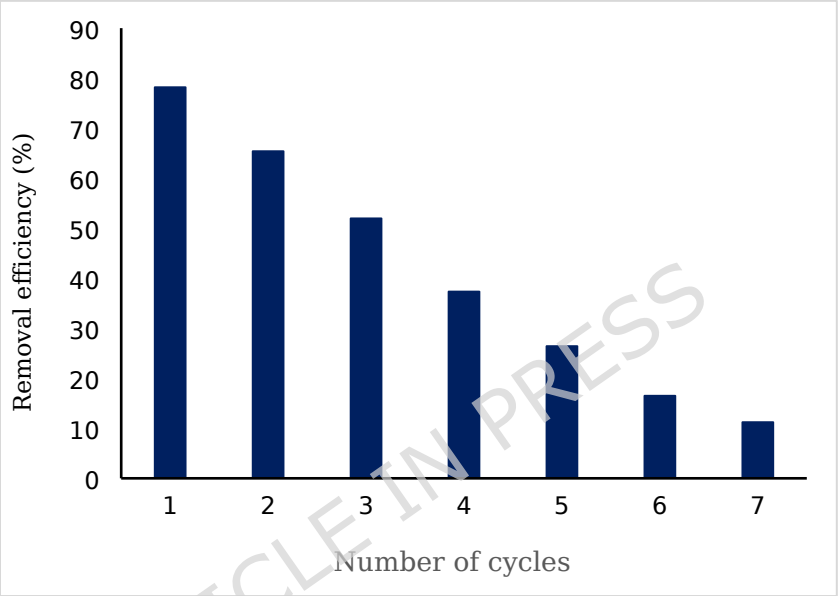

Figure 8. The test of composite adsorbent reusability via the adsorption and desorption recycling process

Environmental sustainability of the treatment process necessitates a clear strategy for the ultimate disposal of the exhausted adsorbent. Once the Fe_3O_4-g-C_3N_4-BC composite reaches its maximum reusability limit, it must be managed carefully to prevent secondary leaching of MB into the environment. A suitable disposal strategy involves thermal mineralization via calcination at temperatures exceeding 500°C, which effectively decomposes the adsorbed organic molecules. Alternatively, the spent composite can be stabilized and immobilized through encapsulation in cementitious matrices for use in non-structural construction applications, providing a safe and circular end-of-life pathway for the material.

4. Conclusions

The adsorbent of the giant grass biochar- Fe_3O_4-g-C_3N_4 composite was successfully synthesized and used for removing MB from water. This adsorbent was characterized by a high fixed carbon content of 55.06%, a low ash content of 4.02%, a reasonably high BET specific surface area of 690 g/m ^{2}, and a desirable SEM morphology featuring cracks and

multiple functional groups. These properties suggest that this material is promising and suitable for various water treatment applications. The maximum MB adsorption reached 93.3% under specific conditions, including an initial MB concentration of 100 mg/L, pH 7, an adsorbent dose of 1.25 g/100 mL, and a contact time of 72.5 minutes. Conversely, the minimum removal efficiency of 71.2% occurred at pH 3, an adsorbent dose of 0.5 g/100 mL, an initial MB concentration of 150 mg/L, and a contact time of 45 min. Adsorption behaviors fitting the Freundlich, Langmuir, Temkin, and Dubinin- Radushkevich models were analyzed under specific experimental conditions. The data aligned best with the Langmuir model (R^2 = 0.99), which assumes single-layer adsorption on a uniform surface with equal binding energy. The dimensionless separation factor (RL) and adsorption intensity (n) further confirmed the highly favorable nature of the interaction. Regarding adsorption kinetics, the data were modeled with intraparticle diffusion, pseudo- first- order, and pseudo- second- order models, with the best fit observed for pseudo- second- order kinetics (R^2 = 0.86). When examining reusability, the adsorption efficiency of the material ranged from 78.2% down to 12.2%. Reusability was limited to the first three cycles, maintaining at least 50% removal, indicating a need for further improvements. Nonetheless, the adsorbent demonstrated high efficiency for MB removal in controlled aqueous solutions, the effects of competing ions and the complexity of actual industrial textile effluents remain to be explored. Future research should focus on pilot- scale applications and developing advanced regeneration techniques to improve the long-term economic viability of the giant grass- derived ternary composite.

Declarations

Ethical Approval

Not applicable

Consent to Participate

Not applicable

Consent to Publish

Not applicable

Acknowledgements

We would like to thank the Environmental Engineering Department at Yildiz Technical University, Esenler, Istanbul, 34220, Turkey, and we are also grateful to the Department of Environmental Engineering, College of Engineering, Sustainable Energy Center of Excellence, Bioprocess and Biotechnology Center of Excellence, Nanotechnology Center of Excellence, Addis Ababa Science and Technology University, 16417 Addis Ababa, Ethiopia.

Finally, we would like to thank the School of Chemical and Metallurgical Engineering, University of the Witwatersrand, 1 Jorissen St, Johannesburg 2000, South Africa

Authors Contributions

All authors contributed to the development of the concept, the preparation of the draft, the revision, and the approval of the submission.

Funding

This project was supported by Horizon Europe research (MSCA,101126655) and TÜBITAK (123C459).

Competing Interests

The authors declare that they have no conflict of interest.

Availability of data and materials.

All data are fully available without restriction from the corresponding authors

References

1. Oyekanmi, A. A., Hanafiah, M. M., Dele-Afolabi, T. T., Ahmad, A. & Alshammari, M. B. Development of nanoparticles loaded composites from agricultural wastes for cationic dye removal from aqueous solution–A review. *J. Environ. Chem. Eng.* **10,** 108263 (2022).

2. Oyekanmi, A. A. *et al.* Sustainable durio zibethinus-derived biosorbents for Congo red removal from aqueous solution: statistical optimization, isotherms and mechanism studies. *Sustainability* **13,** 13264 (2021).

3. Oyekanmi, A. A., Ahmad, A., Hossain, K. & Rafatullah, M. Statistical optimization for adsorption of Rhodamine B dye from aqueous solutions. *J. Mol. Liq.* **281,** 48–58 (2019).

4. Oyekanmi, A. A., Ahmad, A., Hossain, K. & Rafatullah, M. Adsorption of Rhodamine B dye from aqueous solution onto acid treated banana peel: Response surface methodology, kinetics and isotherm studies. *PLoS One* **14,** e0216878 (2019).

5. Shumbe, T. *et al.* Performance Evaluation of a Brewery Wastewater Treatment Plant: A Case of Heineken Brewery, Addis Ababa, Ethiopia. *Heliyon* e40719 (2024).

6. Gebreabe, S. T. *et al.* Response Surface Optimization of Turbidity Removal from

Highly Turbid Surface Water Using Orange Peel Powder as a Sustainable Coagulant. *Next Res.* 101058 (2025).

7. Hu, F. *et al.* Pollution transfer and environmental health implications: network evolution and proximity mechanisms in the Yangtze River Delta, China. *Front. Public Heal.* **14,** (2026).

8. Ahmadi, A., Hajilou, M., Zavari, S. & Yaghmaei, S. A comparative review on adsorption and photocatalytic degradation of classified dyes with metal/non-metal-based modification of graphitic carbon nitride nanocomposites: Synthesis, mechanism, and affecting parameters. *J. Clean. Prod.* **382,** 134967 (2023).

9. Fito, J. *et al.* Adsorption of methylene blue from textile industrial wastewater using activated carbon developed from Rumex abyssinicus plant. *Sci. Rep.* **13,** 1–17 (2023).

10. Al-Omari, A. F., Mahmood, Z. M., Khalaf, A. M. & Fadhil, A. B. Pyrolysis of Quercus cerris kernels for the production of bio-oil and activated biochar for methylene blue adsorption from aqueous phase. *Sustain. Chem. Pharm.* **45,** 102041 (2025).

11. Afshin, S. *et al.* Eco-friendly cost-effective approach for synthesis of ZnO nanoparticles and loaded on worn tire powdered activated carbon as a novel adsorbent to remove organic dyes from aqueous solutions: equilibrium, kinetic, regeneration and thermodynamic study. *Desalin. Water Treat.* **227,** 391–403 (2021).

12. Pourali, P. *et al.* Dissociation of acid blue 113 dye from aqueous solutions using activated persulfate by zero iron nanoparticle from green synthesis: the optimization process with RSM-BBD model: mineralization and reaction kinetic study. *Biomass Convers. Biorefinery* **14,** 6333–6345 (2024).

13. Rajput, P., Yadav, S., Liu, C. & Balasubramanian, P. Predicting biochar adsorption capacity for methylene blue removal using machine learning. *J. Water Process Eng.* **69,** 106749 (2025).

14. Peighambardoust, S. J., Fakhiminajafi, B., Mohammadzadeh Pakdel, P. & Azimi, H. Simultaneous elimination of cationic dyes from water media by carboxymethyl cellulose-graft-poly(acrylamide)/magnetic biochar nanocomposite hydrogel adsorbent. *Environ. Res.* **273,** 121150 (2025).

15. Al-Asadi, S. T. *et al.* A comprehensive review of methylene blue dye adsorption on activated carbon from edible fruit seeds: A case study on kinetics and adsorption models. *Carbon Trends* **20,** 100507 (2025).

16. Pandey, A., Bhagat, A. & Bhaduri, B. Synthesis of magnetite nanoparticles deposited on heat-treated graphitic carbon nitride for the removal of methylene blue dye molecules by adsorption. *Chem. Eng. Commun.* **212,** 922–949 (2025).

17. Navya, B. S. *et al.* Graphene-assisted CuO nanoparticles enhanced the photocatalytic degradation of methylene blue under visible light: Performance and electron transfer mechanisms. *J. Taiwan Inst. Chem. Eng.* 106280 (2025). doi:10.1016/j.jtice.2025.106280

18. Parastar, S. *et al.* Assessment of the efficiency of methylene blue removal from aqueous solutions using Iron magnetic nanoparticles immobilized on clinoptilolite zeolite. *Int. J. Environ. Res.* **19,** 35 (2025).

19. Chen, S. *et al.* Comparison of vacuum ultraviolet-based oxidation as ultrafiltration pretreatment in real water : Performance , risk assessment , and mechanistic insights. *Water Res.* **298,** 125801 (2026).

20. Worku, A. & Tibebu, S. Performance of pilot-scale gravel and sponge bed hydroponic systems vegetated with Duranta erecta treating wastewater in a developing country, Ethiopia, Africa. *Discov. Water* **4,** 21 (2024).

21. Worku, A., Tibebu, S. & Kassahun, E. Phytoremediation Potential of Duranta Erecta in Cascade Hydroponics for Effective Domestic Wastewater Treatment. *Results Eng.* 102837 (2024).

22. Ihsanullah, I. *et al.* Biochar as a sustainable solution for per- and polyfluoroalkyl substances (PFAS) Removal: Progress, Challenges, and Future Horizons. *Sep. Purif. Technol.* **365,** 132674 (2025).

23. Rashtbari, Y. *et al.* Reactive Blue 19 Dye’s Decomposition in Aqueous Environments Using Combined PS/US/AC-Fe3O4 Process. *ChemistrySelect* **10,** e202404801 (2025).

24. Rashtbari, Y. *et al.* The optimization of reactive black 5 dye removal in the sono-catalytic process combined with local yellow montmorillonite and hydrogen peroxide using response surface methodology from aqueous solutions. *Biomass Convers. Biorefinery* **13,** 6067–6081 (2023).

25. Al-Ghouti, M. A. & Da’ana, D. A. Guidelines for the use and interpretation of adsorption isotherm models: A review. *J. Hazard. Mater.* **393,** 122383 (2020).

26. Tibebu, S., Worku, A., Weldmichael, T. G. & Aschale, M. Optimization of biochar production from Rumex abyssinicus using response surface methodology and its

application in amending degraded soil. *Sci. Rep.* (2025).

27. Birhanu, A. *et al.* Optimization of pyrolysis conditions for Catha edulis waste-based biochar production using response surface methodology. *Bioresour. Bioprocess.* **12,** 1–18 (2025).

28. Abdu, M. *et al.* Optimization of photocatalytic degradation of Eriochrome Black T from aqueous solution using TiO2-biochar composite. *Results Eng.* **25,** 104036 (2025).

29. Lobo, W. V., de Souza, L. K. C., Kumar, V. & de Freitas, F. A. Eco-friendly adsorption of Methylene Blue and Remazol Brilliant Blue R from effluents using chemically modified açaí seeds. *Surfaces and Interfaces* **72,** 106970 (2025).

30. Prabakaran, E. & Pillay, K. Synthesis of palm kernel shells-biochar adsorbent for removal of methylene blue and then reused for latent fingerprint detection using spent adsorbent. *Green Anal. Chem.* **13,** 100259 (2025).

31. Kon, D. C. L., Lim, S. F., Chua, D. S. N. & Lim, B. H. Synthesis of coconut husk-derived partially oxidised graphene oxide for methylene blue dye removal. *J. Indian Chem. Soc.* **102,** 101880 (2025).

32. Liu, Z. *et al.* Efficient removal of Congo red and methylene blue using biochar from Medulla Tetrapanacis modified by potassium carbonate. *Bioresour. Technol.* **376,** 128912 (2023).

33. Abdel Azim, E., Samy, M., Hanafy, M. & Mahanna, H. Novel mint-stalks derived biochar for the adsorption of methylene blue dye: Effect of operating parameters, adsorption mechanism, kinetics, isotherms, and thermodynamics. *J. Environ. Manage.* **357,** 120738 (2024).

34. Taib, N. I., Saleh, R., Fisol, A. A., Ismail, I. I. & Ismail, N. N. Adsorptive removal of methylene blue using magnetic graphitic carbon nitride (Fe3O4/g-C3N4) composite: insights into isotherms, kinetics, and thermodynamic properties. *Malaysian J. Anal. Sci.* **29,** 1–16 (2025).

35. Mishra, A. *et al.* Magnetic biochar from marigold floral waste: Synthesis, characterization, and adsorptive removal of methylene blue. *J. Mol. Struct.* **1341,** 142657 (2025).

36. Guo, F. *et al.* Efficient removal of methylene blue via two-step modification hazelnut shell biochar: Process intensification, kinetics and thermodynamics. *J. Ind. Eng.*

Chem. **125,** 105–116 (2023).

37. Essa, R. A., El-Aal, M. A., Sedky, A., Abo Zeid, E. F. & Amin, S. ZnO NPs-modified biochar derived from banana peels for adsorptive removal of methylene blue from water. *J. Mol. Struct.* **1321,** 139821 (2025).

38. Xiao, Y. *et al.* Graphitic carbon nitride/biochar composite synthesized by a facile ball-milling method for the adsorption and photocatalytic degradation of enrofloxacin. *J. Environ. Sci. (China)* **103,** 93–107 (2021).

39. Tibebu, S., Worku, A. & Weldmichael, T. G. Potential of biochar g-C_3N_4 nanocomposites in soil remediation of 2, 4-D with mechanistic insights and future prospects. *Discov. Environ.* **3,** 1–18 (2025).

40. Tibebu, S. *et al.* Efficient photocatalytic degradation of methylene blue using Arundo donax biochar/graphitic carbon nitride composite. *Results Eng.* 108143 (2025).

41. Lalmalsawmdawngliani, Lalhriatpuia, C. & Tiwari, D. Biochar-derived nanocomposites for environmental remediation: The insights and future perspectives. *J. Environ. Chem. Eng.* **12,** 111840 (2024).

42. Cai, F. *et al.* Preparation of nitrogen-doped bagasse-derived biochar with outstanding methylene blue adsorption performance. *Ind. Crops Prod.* **224,** 120415 (2025).

43. Fan, W. & Zhang, X. Magnetic coconut shell biochar/sodium alginate composite aerogel beads for efficient removal of methylene blue from wastewater: Synthesis, characterization, and mechanism. *Int. J. Biol. Macromol.* **284,** 137945 (2025).

44. Tibebu, S. *et al.* The application of Rumex Abysinicus derived activated carbon/bentonite clay/graphene oxide/iron oxide nanocomposite for removal of chromium from aqueous solution. *Sci. Rep.* **14,** 19280 (2024).

45. Zhu, X. *et al.* Thermal treatment of biochar in the air/nitrogen atmosphere for developed mesoporosity and enhanced adsorption to tetracycline. *Bioresour. Technol.* **263,** 475–482 (2018).

46. Wang, Z. *et al.* Facile synthesis of carbon-rich g-C3N4 by copolymerization of urea and tetracyanoethylene for photocatalytic degradation of Orange II. *J. Photochem. Photobiol. A Chem.* **358,** 61–69 (2018).

47. Mahdavian, F. *et al.* Enhanced removal of cefixime from aqueous solutions using Fe3O4@ GO nanocomposite with ultrasonic: isotherm and kinetics study. *Desalin. Water Treat.* **280,** 224–239 (2022).

48. Nguyen, T. H. M., Nguyen, V. C. & Nguyen, T. H. A. Photo-reduced synthesis of a Z-scheme Ag@Fe3O4/g-C3N4 composite for photoreduction of 4-nitrophenol and photocatalytic activity. *Brazilian J. Chem. Eng.* (2025). doi:10.1007/s43153-025-00536-5

49. Tibebu, S. *et al.* Cr (VI) removal from aqueous solutions using Cordia Africana-based activated carbon/red clay/magnetite nanocomposite: optimization via one factor at a time and response surface methodology. *Biomass Convers. Biorefinery* 1–27 (2025).

50. Nure, J. F., Shibeshi, N. T., Asfaw, S. L., Audenaer, W. & Van Hulle, S. W. H. COD and colour removal from molasses spent wash using activated carbon produced from bagasse fly ash of matahara sugar factory, Oromiya region, Ethiopia. *Water SA* **43,** 470–479 (2017).

51. Fito, J., Tibebu, S. & Nkambule, T. T. I. Optimization of Cr (VI) removal from aqueous solution with activated carbon derived from Eichhornia crassipes under response surface methodology. *BMC Chem.* **17,** 1–19 (2023).

52. Fito, J., Abrham, S. & Angassa, K. Adsorption of Methylene Blue from Textile Industrial Wastewater onto Activated Carbon of Parthenium hysterophorus. *Int. J. Environ. Res.* **14,** 501–511 (2020).

53. Anuradha, C. S., Devi, C. S., Haritha, R., Varma, M. V. M. & Sree, M. H. M. Facile Green Synthesis and Photocatalytic Efficiency of Ag-Zn Bimetallic Nanoparticles for Degradation of Methylene Blue.

54. Bayça, F. Molecular adsorption mechanism of methylene blue dye on ulexite. *Sci. Rep.* (2026).

55. Oumirdine, A. *et al.* Adsorptive removal of methylene blue and malachite green onto a natural Comorian clay: physicochemical properties, optimization, adsorption isotherms, kinetics, and mechanisms. *Inorg. Chem. Commun.* 116425 (2026).

56. Tibebu, S. *et al.* Synthesis Optimization of Activated Carbon Driven from Scrap Tire for Adsorbent Yield and Methylene Blue Removal under Response Surface Methodology. *Adv. Mater. Sci. Eng.* **2022,** em0097 (2022).

57. Pourali, P. *et al.* Loading of zinc oxide nanoparticles from green synthesis on the low cost and eco-friendly activated carbon and its application for diazinon removal: isotherm, kinetics and retrieval study. *Appl. Water Sci.* **13,** 101 (2023).

58. Ashebir, H. *et al.* Advanced methylene blue adsorption with a tailored

biochar/graphene oxide/magnetite nanocomposite: characterization, optimization, and reusability. *Biomass Convers. Biorefinery* **15,** 15885–15906 (2025).

59. Ashebir, H., Nure, J. F., Worku, A. & Msagati, T. A. M. Prosopis juliflora biochar for adsorption of sulfamethoxazole and ciprofloxacin from pharmaceutical wastewater. *Desalin. Water Treat.* **320,** 100691 (2024).

60. Boumezough, Y., Arris, S., Carabineiro, S. A. C. & Viscusi, G. Optimized removal of methylene blue using chemically activated and thermally modified Opuntia ficus-indica bioadsorbent: a response surface methodology approach. *Biomass Convers. Biorefinery* **15,** 17427–17444 (2025).

61. Teweldebrihan, M. D., Gnaro, M. A. & Dinka, M. O. The application of magnetite biochar composite derived from parthenium hysterophorus for the adsorption of methylene blue from aqueous solution. *Front. Environ. Sci.* **12,** 1375437 (2024).

62. Lopez, E. C. R. *et al.* Rapid removal of methylene blue in water using polymer-based biochar nanocomposite-coated filters. *Solid State Phenom.* **324,** 116–124 (2021).

63. Cheng, Z. *et al.* Ultrasound-assisted heterogeneous Fenton-like process for methylene blue removal using magnetic MnFe2O4/biochar nanocomposite. *Appl. Surf. Sci.* **566,** 150654 (2021).

64. Basaleh, A. A., Al-Malack, M. H. & Saleh, T. A. Methylene Blue removal using polyamide-vermiculite nanocomposites: Kinetics, equilibrium and thermodynamic study. *J. Environ. Chem. Eng.* **7,** 103107 (2019).

65. Li, Z. *et al.* Fabrication of novel sandwich nanocomposite as an efficient and regenerable adsorbent for methylene blue and Pb (II) ion removal. *J. Environ. Manage.* **218,** 363–373 (2018).

66. Yu, F. *et al.* ZnO/biochar nanocomposites via solvent free ball milling for enhanced adsorption and photocatalytic degradation of methylene blue. *J. Hazard. Mater.* **415,** 125511 (2021).

67. Kazemi, M. S. & Sobhani, A. CuMn2O4/chitosan micro/nanocomposite: Green synthesis, methylene blue removal, and study of kinetic adsorption, adsorption isotherm experiments, mechanism and adsorbent capacity. *Arab. J. Chem.* **16,** 104754 (2023).

68. Eltaweil, A. S., Abdelfatah, A. M., Hosny, M. & Fawzy, M. Novel biogenic synthesis of a Ag@ Biochar nanocomposite as an antimicrobial agent and photocatalyst for

methylene blue degradation. *ACS omega* **7,** 8046–8059 (2022).